Central Lancashire Online Knowledge (CLoK)

Title	Satellite attitude identification and prediction based on neural network compensation
Type	Article
URL	https://clok.uclan.ac.uk/id/eprint/45368/
DOI	10.34133/space.0009
Date	2023
Citation	Sun, Zibin, Simo, Jules and Gong, Shengping (2023) Satellite attitude identification and prediction based on neural network compensation. Space: Science & Technology.
Creators	Sun, Zibin, Simo, Jules and Gong, Shengping

RESEARCH ARTICLE

Satellite Attitude Identification and Prediction Based on Neural Network Compensation

Zibin Sun[1], Jules Simo[2], and Shengping Gong[3*]

[1]School of Aerospace Engineering, Tsinghua University, Beijing 100084, China. [2]School of Engineering, University of Central Lancashire, Preston PR1 1XJ, UK. [3]School of Astronuatics, Beihang University, Beijing 102206, China.

*Address correspondence to: gongsp@buaa.edu.cn

This paper proposed a new attitude determination method for low-orbit spacecraft. The attitude prediction accuracy is greatly improved by adding the unmodeled environmental torque to the dynamic equation. Specifically, the environmental torque extraction algorithm based on extended Kalman filter and series extended state observer is introduced, and the unmodeled part of dynamic is identified through the inverse dynamic model. Then, the collected data are analyzed and trained by a backpropagation neural network, resulting in an attitude-torque mapping network with compensation ability. The simulation results show that the proposed feedback attitude prediction algorithm can outperform standard methods and provide a high accurate picture of prediction and reliability with discontinuous measurement.

Introduction

The attitude determination of low-Earth-orbit (LEO) satellite is essential for the normal operation such as communication, maneuver, telemetry, etc. Under normal circumstances, the satellite is equipped with infrared Earth sensors and star sensors, which can achieve precise attitude determination in real time. However, at the end of the satellite service life, or serious malfunctions that occur in satellite electronic system, the attitude determination system is unable to function properly. Then, it is necessary to descend the orbit for the ablation and disorganization in the atmosphere. During this process, accurate satellite attitude prediction without the assistance of sensors is very critical, which can help to determine the condition of satellite debris, estimate the landing area, and reduce the damage caused by debris in advance.

Since the 1960s, researchers have been constantly exploring how to estimate the orientation of nonworking LEO satellite. There are 2 main research interests: The first is to refine the environmental torque model, including the gravitational gradient torque [1–3], magnetic torque [4], aerodynamic torque [5–7], etc. The offline attitude estimation accuracy and credible period have been greatly improved with the meticulous environment model. The second method is based on filtering and optimizing the measurement results observed by ground facilities. Many data processing algorithms including the modified Kalman filter [8], spatial-based least-squares estimation [9], multiple model adaptive estimation [10], centered error entropy unscented Kalman filter [11], the predictive attitude determination algorithm [12], etc. are used to filter out the observation noise tangled in the data. These data filtering algorithms have been successfully validated on multiple aircraft platforms [13–16].

The disadvantages of the above aforementioned techniques are also evident. The method based on refined environment model can estimate the effect precisely in a period of time, but the reliability wound descends greatly due to the uncertainty of aerodynamic model and satellite parameters. On the other hand, the method based on data filtering and optimization can obtain accurate observations in real time, but it is difficult to combine the prediction algorithm with the dynamic model to form a prediction framework due to the high nonlinearity and coupling of the environmental torques.

Recently, the breakthrough in neural network recently provides possibility for accurate attitude prediction. The neural network is a nonlinear mapping function with high generalization ability and self-learning ability. It has been proved mathematically that the network structure with enough neurons can estimate any nonlinear function with extremely high accuracy [17]. The combination of neural network and dynamic model has been applied to the fields of aerospace, machinery, and intelligent control. Lin et al. combine the fuzzy intelligence control with neural network to achieve the attitude control of a solar sail [18]. Carrara develops a neural-network-based attitude controller of a satellite with deployable solar arrays [19]. Zhang et al. utilize neural network to adjust the parameters of proportional integral derivative control of satellite efficiently [20]. Raja et al. implement an adaptive neural network with quaternion and Euler angles for the optimization of proportional integral derivative satellite attitude dynamics and control system [21]. Yun and Fan propose an adaptive control method based on Radial Basis Function (RBF) neural network to solve the problem of satellite attitude tracking [22]. However, the above methods only propose theory and simulation experiment, without actual data as verification, and do not consider the measurement noise, which reduces the reliability in practical applications.

The main contributions of this paper are as follows: First, a feedback attitude prediction algorithm is proposed, which can achieve the current and persistent attitude prediction with high accuracy. The complex dynamic model, few short-term attitude observation data, and extremely uncertain atmospheric torque cause it difficult to determine the attitude. However, our methods can extract the high-order unmodeled dynamics from the attitude data and then compensate the environment uncertainty through a trained neural network. Second, a high-order torque identification framework based on extended Kalman filter (EKF) and series extended state observer (ESO) is proposed, which can reduce observation noise and effectively extract uncertain environmental torque. The proposed framework can well solve the deficiency of conventional ESO observation in noncascade system and combine Kalman filter to reduce the observation error. Through the combination of the 2 contributions, a set of highly portable spacecraft attitude and orbit prediction framework is provided.

The organization of this paper proceeds as follows: In the Attitude Prediction Model of LEO Satellite section, the environmental torques considered in LEO are reviewed, and the attitude kinematic and dynamic model based on quaternion are introduced. Then, the unmodeled torque extraction algorithm based on EKF and series ESO is proposed in the Filtering and Determination Attitude section. A well-trained torque compensation network is introduced in the Unmodeled Compensation Based on Neural Network section, which can map the current state to the unmodeled environment torque. In the Simulation and Results section, simulation results based on an actual satellite are presented to illustrate the effectiveness of the proposed algorithm. The results show that the method can reduce the attitude prediction error effectively and maintain the reliability of the estimation at a high level with persistent on-line measurement.

Attitude Prediction Model of LEO Satellite

For falling spacecrafts in LEO, the main environmental disturbances are the gravitational gradient torque generated by gravity and the aerodynamic torque generated by atmospheric drag. Under the interference of these environmental torques, the spacecraft velocity and angular velocity also change, further affecting the prediction of the meteorite trajectory. This section reviews the environmental torque considered in LEO and, furthermore, demonstrates the kinematic and dynamic framework of attitude prediction based on quaternion. The transformation between the Euler angle and quaternion is also presented.

Environmental torque of LEO satellites

LEO satellites are affected by various environmental torques, including gravity gradient torque, aerodynamic torque, solar radiation torque, magnetic torque, etc. The torques are related to satellite and environment conditions, such as the size, mass, mass distribution, and orbital height that are essential for the attitude prediction of the uncontrolled satellite. For LEO spacecrafts, the aerodynamic torque and gravity gradient torque are mainly considered. The gravity gradient torque is often utilized to stabilize Earth pointing with several degrees of error. The aerodynamic torque plays a dominant role in the LEO and will interfere the control system, causing the spacecraft to reverse at the end of the mission.

According to the law of gravitation, the gravity of Earth decreases with the distance from the center of Earth. So, the

gravity of each part of the satellite is also different, resulting in the gravity gradient torque. The gravity gradient torque can be described as [23]:

$$N_{GG} = \frac{3\mu}{\|\mathbf{r}\|^5}[\mathbf{r} \times (\mathbf{J} \cdot \mathbf{r})] \tag{1}$$

where $\mathbf{r}$ represents the centroid position vector of satellite relative to Earth, $\mathbf{J}$ is the inertia matrix of satellite, and μ is the gravitational constant of Earth. For LEO satellites, if the inertia matrix is on the order of 1000 kg m^2, then the gravity gradient torque is around 3×10^{-3} N m [23].

The aerodynamic torque is generally caused by the impact of atmospheric molecules on the surface of spacecraft. The complex space shape leads to different aerodynamic forces on different sides of the asymmetric satellite, resulting in the aerodynamic torque. The aerodynamic torque is related to many elements, including the current altitude, velocity, windward area, and so on. Since it is difficult to calculate the windward area in real time, wind tunnel tests are usually carried out to obtain the aerodynamic coefficients under different attitudes. Then, the aerodynamic torque is determined according to the angle of attack and sideslip angle in the prediction. The aerodynamic torque can be described as [23]:

$$\mathbf{N}aero = \frac{1}{2}\mathbf{C_D}S_{ref}\rho v^2 r_{cp-cm} \tag{2}$$

where $\mathbf{C_D}$ represents the aerodynamic torque coefficients in 3 directions in body coordinate system, S_{ref} is the reference windward area, ρ represents the atmosphere density, v is the velocity of the satellite, and r_{cp-cm} is the offset distance between the satellite centroid and the pressure center. The coefficient matrix is obtained in real time by calculating the attack angle and sideslip angle. Considering a satellite with 300 km orbital altitude, 7.7 km/s velocity, 5×10^{-11} kg/m^3 atmospheric density, 1 m^2 windward area and 1 m pneumatic arm, then the aerodynamic torque is around 3×10^{-3} N m at the same level as the gravity gradient torque [23].

As for magnetic torque and solar radiation torque, for ordinary LEO satellites, the magnitude of both is around 1×10^{-5} N m, which is too small compared with the gravity gradient torque and the aerodynamic torque. Therefore, the magnetic torque and the solar radiation torque are not considered in this paper [23].

Attitude kinematic and dynamic equations

The attitude of satellite is usually defined by the rotation between the Earth-centered inertial system and the body-fixed frame. The Euler angle rotation sequence used in this paper is yaw–pitch–roll. On the basis of the above definition, the attitude kinematic equation in the Euler angle form is given by:

$$\begin{cases} \dot{\varphi} = \dfrac{1}{\cos\theta}\left(\omega_{xb}\sin\theta\sin\varphi + \omega_{xb}\cos\theta + \omega_{zb}\cos\varphi\sin\theta\right) \\[2mm] \dot{\theta} = \omega_{yb}\cos\varphi - \omega_{zb}\sin\varphi \\[2mm] \dot{\psi} = \dfrac{1}{\cos\theta}\left(\omega_{yb}\sin\varphi + \omega_{zb}\cos\varphi\right) \end{cases} \tag{3}$$

where ψ, θ, and φ represent the yaw, pitch, and roll angle, $\boldsymbol{\omega b} = [\omega_{xb}, \omega_{yb}, \omega_{zb}]^{\mathrm{T}}$ is the angular velocity expressed in body-fixed frame. It is worth noting that in some special attitudes

(the pitch angle is 90°), the attitude kinematic equation expressed by the Euler angles (Eq. 3) will cause singularities. Here, we use quaternions to express the attitude kinematic equation as:

$$
\begin{bmatrix} \dot{q}_0 \\ \dot{q}_1 \\ \dot{q}_2 \\ \dot{q}_3 \end{bmatrix} = \frac{1}{2} \begin{bmatrix} 0 & -\omega_{xb} & -\omega_{yb} & -\omega_{zb} \\ \omega_{xb} & 0 & \omega_{zb} & -\omega_{yb} \\ \omega_{yb} & -\omega_{zb} & 0 & \omega_{xb} \\ \omega_{zb} & \omega_{yb} & -\omega_{xb} & 0 \end{bmatrix} \cdot \begin{bmatrix} q_0 \\ q_1 \\ q_2 \\ q_3 \end{bmatrix} \tag{4}
$$

The main advantage of the quaternion representation is that the attitude kinematic equation is free of singularities and the kinematic equation matrix is linear. In addition, the conversion between the quaternion and the Euler angle can be written as:

$$
\begin{aligned}
\varphi &= \arcsin\left(2\left(q_2 q_3 + q_0 q_1\right)\right) \\
\theta &= \arctan \frac{-2\left(q_1 q_2 - q_0 q_3\right)}{q_0^2 - q_1^2 + q_2^2 - q_3^2} \\
\psi &= \arctan \frac{-2\left(q_1 q_3 - q_0 q_2\right)}{q_0^2 - q_1^2 - q_2^2 + q_3^2}
\end{aligned}
\tag{5}
$$

$$
q = \begin{bmatrix} \cos\frac{\varphi}{2}\cos\frac{\theta}{2}\cos\frac{\psi}{2} + \sin\frac{\varphi}{2}\sin\frac{\theta}{2}\sin\frac{\psi}{2} \\ \sin\frac{\varphi}{2}\cos\frac{\theta}{2}\cos\frac{\psi}{2} - \cos\frac{\varphi}{2}\sin\frac{\theta}{2}\sin\frac{\psi}{2} \\ \cos\frac{\varphi}{2}\sin\frac{\theta}{2}\cos\frac{\psi}{2} + \sin\frac{\varphi}{2}\cos\frac{\theta}{2}\sin\frac{\psi}{2} \\ \cos\frac{\varphi}{2}\cos\frac{\theta}{2}\sin\frac{\psi}{2} - \sin\frac{\varphi}{2}\sin\frac{\theta}{2}\cos\frac{\psi}{2} \end{bmatrix} \tag{6}
$$

As for the attitude dynamics, the angular momentum of the spacecraft can be expressed as:

$$
\mathbf{H} = \mathbf{J}\boldsymbol{\omega}_b \tag{7}
$$

According to the angular momentum theorem, the change rate of the spacecraft angular momentum can be expressed as:

$$
\frac{d\mathbf{H}}{dt} = \mathbf{M} \tag{8}
$$

The above equation holds in any coordinate system, while the inertia matrix changes with the rotation of the spacecraft in the Earth-centered inertial system, which is difficult for the attitude integral prediction. In general, the attitude dynamic equation is usually expressed in the body fixed frame as:

$$
\mathbf{J} \cdot \dot{\boldsymbol{\omega}}_b + \boldsymbol{\omega}_b \times \left(\mathbf{J} \cdot \boldsymbol{\omega}_b\right) = \mathbf{M} \tag{9}
$$

where $\mathbf{M}$ represents the sum of environmental moments.

Filtering and Determination of Attitude

In the open-loop prediction, the accurate measurement of satellite attitude is very important. A tiny initial deviation will cause the prediction results to gradually deviate from the actual condition. The most straightforward method to estimate the satellite attitude for a long time is to combine the dynamic model with the observation data and then calculate the optimal estimation according to the principle of minimum variance. After obtaining the attitude estimation, the high-order unmodeled information can be extracted from the original data through the extended state identification, which will be instrumental to refine the dynamic model. In this section, the estimation results of the satellite state are obtained by the EKF, and then the unmodeled torque of satellite is estimated by series of the ESO.

Extended Kalman filter

The attitude data measured by the ground observation facility have uncertain Gaussian noise, which brings trouble to high precise attitude determination. The EKF can integrate attitude measurement data and prediction system by updating the optimal estimation of the satellite attitude online according to the real-time observation. In this section, the satellite attitude is expressed as a quaternion vector, and the more accurate attitude estimation is obtained by a standard EKF process. Consider the nonlinear prediction update shown by:

$$
\widehat{\mathbf{x}}_{k+1}^- = \widehat{\mathbf{x}}_k + \mathbf{f}\left(\widehat{\mathbf{x}}_k\right)\Delta t \tag{10}
$$

where $\mathbf{f}\left(\widehat{\mathbf{x}}_k\right)$ represents the sum of nonlinear environment torque at state $\widehat{\mathbf{x}}_k$ and Δt represents the step size of EKF. Assuming that the covariance matrix of the current state is $\mathbf{P}_k$ and then the update of the covariance matrix is given by:

$$
\mathbf{P}_{k+1}^- = \boldsymbol{\Phi}_{k+1}\mathbf{P}_k\boldsymbol{\Phi}_{k+1}^{\mathrm{T}} + \mathbf{Q}_{k+1} \tag{11}
$$

where $\mathbf{Q}$ represents the system process noise covariance matrix and $\boldsymbol{\Phi}_k$ is the state-transition matrix and can be expressed in the following form:

$$
\boldsymbol{\Phi}_k = \frac{1}{2}\begin{bmatrix} 2\Delta t & -\omega_{xk} & -\omega_{yk} & -\omega_{zk} & -q_{1k} & -q_{2k} & -q_{3k} \\ \omega_{xk} & 2\Delta t & \omega_{zk} & -\omega_{yk} & q_{0k} & -q_{3k} & q_{2k} \\ \omega_{yk} & -\omega_{zk} & 2\Delta t & \omega_{xk} & q_{3k} & q_{0k} & -q_{1k} \\ \omega_{zk} & \omega_{yk} & -\omega_{xk} & 2\Delta t & -q_{2k} & q_{1k} & q_{0k} \\ 0 & 0 & 0 & 0 & 2\Delta t & 0 & 0 \\ 0 & 0 & 0 & 0 & 0 & 2\Delta t & 0 \\ 0 & 0 & 0 & 0 & 0 & 0 & 2\Delta t \end{bmatrix} \tag{12}
$$

The Kalman gain update equation is defined as:

$$
\mathbf{K}_{k+1} = \mathbf{P}_{k+1}^- \mathbf{H}_{k+1}^{\mathrm{T}}\left(\mathbf{H}_{k+1}\mathbf{P}_{k+1}^- \mathbf{H}_{k+1}^{\mathrm{T}} + \mathbf{R}_{k+1}\right)^{-1} \tag{13}
$$

where $\mathbf{R}$ represents the measurement noise covariance matrix and $\mathbf{H}_k$ is the measurement matrix, and for simplicity of calculation, we have:

$$\mathbf{H}_k = \begin{bmatrix} 1 & 0 & 0 & 0 \\ 0 & 1 & 0 & 0 \\ 0 & 0 & 1 & 0 \\ 0 & 0 & 0 & 1 \end{bmatrix} \tag{14}$$

Then, the state and the covariance matrix update based on Kalman gain can be expressed as:

$$\widehat{\mathbf{x}}_{k+1} = \widehat{\mathbf{x}}_{k+1}^- + \mathbf{K}_k\left(\mathbf{y}_{k+1} - \mathbf{H}\widehat{\mathbf{x}}_{k+1}^-\right) \tag{15}$$

$$\mathbf{P}_{k+1} = \left[\mathbf{I} - \mathbf{K}_{k+1}\mathbf{H}_{k+1}\right]\mathbf{P}_{k+1}^-\left[\mathbf{I} - \mathbf{K}_{k+1}\mathbf{H}_{k+1}\right]^{\mathrm{T}} + \mathbf{H}_{k+1}\mathbf{R}_{k+1}\mathbf{H}_{k+1}^{\mathrm{T}} \tag{16}$$

where $\mathbf{y}_k = \mathbf{H}\widehat{\mathbf{x}}_k$ represents the measurement results at t_k.

Remark. *It is worth noting that in the process of EKF, the process noise and measurement noise must meet the conditions of the linear uncorrelation, the zero mean, and Gaussian distribution; otherwise, the filtering result may be inaccurate.*

Series ESO

Some status information is difficult to be measured directly by the sensors in the field of engineering, such as angular velocity, angular acceleration, etc. However, the uncertainty estimation, including the internal coupling, the external unknown disturbances, and the unmodeled dynamics, can be determined with rarely observation information by building an ESO. After obtaining the optimal attitude estimation with the EKF, a series of ESO is introduced to extract the high-order unmodeled information hiding in the attitude. Consider the following nonlinear dynamic system to be observed:

$$\begin{cases} \dot{\mathbf{q}} = A(\boldsymbol{\omega})\mathbf{q} \\ J\dot{\boldsymbol{\omega}} = -\boldsymbol{\omega}\times J\boldsymbol{\omega} + f(\mathbf{q},\mathbf{s}) + \mathbf{d} \end{cases} \tag{17}$$

where $\mathbf{q} = [q_0, q_1, q_2, q_3]^{\mathrm{T}}$ represents the attitude quaternion, $f(\mathbf{q},\mathbf{s})$ is the known as high-order input, which stands for the known environment torques of satellite based on orbit information $\mathbf{s}$, and d is the unknown disturbance to be identified. A series ESO system $\widehat{\mathbf{d}} = \boldsymbol{\Phi}_b(\boldsymbol{\Phi}_a(\mathbf{q}))$ is constructed to obtain the best estimation of $\mathbf{d}$. The internal observer is designed as follows:

$$\boldsymbol{\Phi}_a: \begin{cases} e_1 = z_{a1} - y_1 \\ \dot{z}_{a1} = z_{a2} - \beta_{a1}e_1 \\ \dot{z}_{a2} = -\beta_{a2}fal(e_1, 0.5, \delta) \end{cases} \tag{18}$$

where $y_1 \in q_i + v_i(i = 0, 1, 2, 3)$ represents the attitude measurement results based on the sensors and the ground observation facility, v_i is the measurement noise, $\beta_a = [\beta_{a1}, \beta_{a2}] > 0$ is the
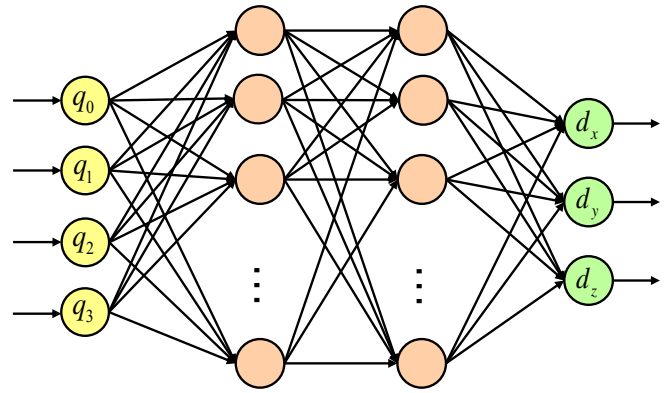

Fig. 1. The structure of attitude prediction BP network.

feedback coefficient, $\mathbf{z}_a = [z_{a1}, z_{a2}]^T$ is the observer system state, and the nonlinear error correction function is given by:

$$fal(\varepsilon, \alpha, \delta) = \begin{cases} |\varepsilon|^\alpha sgn(\varepsilon), \; |\varepsilon| > \delta \\ \varepsilon/\delta^{1-\alpha}, \; |\varepsilon| \le \delta \end{cases} \tag{19}$$

The estimated value of the quaternion derivative can be expressed as: $\mathbf{z}_{a2} = \widehat{\dot{\mathbf{q}}}$, and the estimation results of the angular velocity is obtained through the reverse process of Eq. 4 as:

$$\begin{bmatrix} \widehat{\boldsymbol{\omega}} \\ 0 \end{bmatrix} = 2\begin{bmatrix} -q_1 & -q_2 & -q_3 & 0 \\ q_0 & -q_3 & q_2 & 0 \\ q_3 & q_0 & -q_1 & 0 \\ -q_2 & q_1 & q_0 & 1 \end{bmatrix}^{-1} \cdot \widehat{\dot{\mathbf{q}}} \tag{20}$$

The internal ESO has been completed up to now. The angular velocity information of the satellite system can be extracted from the observed quaternion data through the internal ESO, and the angular velocity can be more accurate through a low-pass filter. The external observer is designed as follows:

$$\boldsymbol{\Phi}_b: \begin{cases} e_2 = z_{b1} - y_2 \\ \dot{z}_{b1} = z_{b2} - \beta_{b1}e_2 \\ \dot{z}_{b2} = -\beta_{b2}fal(e_2, 0.25, \delta) \end{cases} \tag{21}$$

where $y_2 \in \widehat{\omega}_i(i = 1, 2, 3)$ represents the angular velocity estimation results based on the internal ESO, $\beta_b = [\beta_{b1}, \beta_{b2}] > 0$ is the feedback coefficient, $\mathbf{z}_b = [z_{b1}, z_{b2}]^T$ is the observer system state, and $z_{b2} = \widehat{\dot{\omega}}_i$ is the estimation result of angular velocity derivative. Then, the estimation result of environment torques can be obtained through the inverse process of Eq. 17 as:

$$\widehat{\mathbf{d}} = \widehat{\boldsymbol{\omega}} \times J\widehat{\boldsymbol{\omega}} - J\widehat{\dot{\boldsymbol{\omega}}} - f(\widehat{\mathbf{q}}, \mathbf{s}) \tag{22}$$

Similar to the internal ESO, the high-frequency oscillation generated in the estimation process can be suppressed by designing a low-pass filter.

Unmodeled Compensation Based on Neural Network

In this section, a double hidden layer backpropagation (BP) network is constructed to learn the unmodeled environment torque in the satellite. The BP neural network has high generalization and self-learning ability, can reconstruct the mapping relationship between the state and the environmental torque, and plays a critical role in attitude prediction system.

Considering a 3-layer neural network as shown in Fig. 1, the input layer of the network is the measured attitude information: $x_{input} = [q_0, q_1, q_2, q_3]^T$, and the tutor signal of supervised learning is the unmodeled torque identified in the Filtering and Determination of Attitude section: $y = [d_1, d_2, d_3]^T$. The activation function of the first hidden layer is the "Relu" function defined as:

Fig. 2. The whole training process of the neural network.

$$Relu: f_1(s) = \begin{cases} s & s > 0 \\ 0 & s \leq 0 \end{cases} \tag{23}$$

Then, the relationship between the first input and output layer can be expressed as:

$$x_i^{(2)} = f_1\left(s_i^{(1)}\right) = f_1\left(\sum_{j=0}^{N_1-1} w_{ij}^{(1)} x_j^{(1)}\right) \quad i = 1, 2, \ldots, N_1 \tag{24}$$

where $N_{(q)}, q = 1, 2, 3$ represents the number of neurons in each layer and $x_0 = 1$ represents the bias term, which is not displayed in Fig. 2 for the intuition. The activation function of the second hidden layer is a "Sigmoid" function defined as:

$$Sigmoid: f(s) = \frac{1}{1 + e^{-s}} \tag{25}$$

Then, the relationship between the second input and output layer can be expressed as:

$$x_i^{(3)} = f_2\left(s_i^{(2)}\right) = f_2\left(\sum_{j=0}^{N_2-1} w_{ij}^{(2)} x_j^{(2)}\right) \quad i = 1, 2, \ldots, N_2 \tag{26}$$

The final output of neural network is shown as:

$$y_i = \sum_{j=0}^{N_3-1} w_{ij}^{(3)} x_j^{(3)} \quad i = 1, 2, 3 \tag{27}$$

The above process denotes the forward propagation of a single group of samples. For the N groups of measured samples, $\mathbf{x}_{input} = [\mathbf{q}_1, \mathbf{q}_2, \ldots, \mathbf{q}_N]$, and the tutor signal: $\mathbf{y}_{target} = [\mathbf{d}_1, \mathbf{d}_2, \ldots, \mathbf{d}_N]$. The loss function based on sample set is selected as:

$$E = \frac{1}{2} \sum_{p=1}^{N} \left(\widehat{\mathbf{d}}_\mathbf{p} - \mathbf{d}_\mathbf{p}\right)^2 = \frac{1}{2} \sum_{p=1}^{N} E_p \tag{28}$$

Table. The initial orbit and attitude parameters of Tiangong-1 Space Station.

Mass (kg)	7,661.4
Attitude angle (°)	91, −59, −137
Angular velocity (°/s)	−0.2679, −0.01085, 1.0207
Position (km, in J2000)	4,561.4433, −3,977.5169, −2,366.0892
Velocity (km/s, in J2000)	5.3239 3.3147 4.6915
Inertia matrix (kg m²)	$\begin{bmatrix} 16,407.00 & -132.87 & 448.55 \\ -132.87 & 76,391.94 & -27.54 \\ 448.55 & -27.54 & 70,912.02 \end{bmatrix}$

During the process of the network learning, the weight is constantly updated according to the error between the output **y** and the tutor signal **y**$_{target}$. For the qth layer:

$$\frac{\partial E_p}{\partial w_{ij}^{(q)}} = \frac{\partial E_p}{\partial x_{pi}^{(q)}} \frac{\partial x_{pi}^{(q)}}{\partial s_{pi}^{(q)}} \frac{\partial s_{pi}^{(q)}}{\partial w_{ij}^{(q)}} \qquad (29)$$

$$= -\left(d_{pi} - x_{pi}^{(q)}\right) f_q'\left(s_{pi}^{(q)}\right) x_{pj}^{(q-1)}$$

By analogy, the result of $\frac{\partial E_p}{\partial w_{ij}^{(q)}}$, $q = 1, 2, 3$ is calculated continuously by backward propagation. Then, the update of each neuron weights can be expressed as:

$$w_{ij}^{(q)}(k+1) = w_{ij}^{(q)}(k) + \alpha \frac{\partial E_p}{\partial w_{ij}^{(q)}} \qquad (30)$$

where $\alpha > 0$ is the network learning rate. The whole training process is shown in Fig. 2.

Remark. The normalization of the network is essential. Since the magnitude of the identified environmental torque is too small, the training set should be mapped to the range of [0,1] by normalization for a better training efficiency. The corresponding linear transformation is also required during verification of the test set and the attitude prediction process.

Simulation and Results

In this section, the whole process and simulation results of the prediction system are presented. The target spacecraft is selected as Tiangong-1 Space Station descending into the atmosphere.
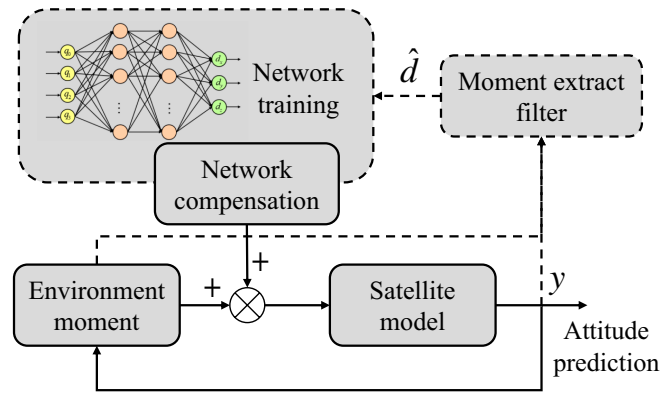

Fig. 3. The structure of attitude prediction system.

The detailed parameters are shown in Table. Because of the coupling effect of the spacecraft orbit and attitude, it is difficult to consider the independent influence of the environmental torque independently. Therefore, 13 state parameters including a 3-axis position, a 3-axis velocity (both expressed in J2000 coordinate system), a quaternion, and an angular velocity are used in the simulation. A disturbance is artificially added to the simulation as the unmodeled environmental torque. The time step of the EKF is 0.1 s, and the covariance matrix of the observation noise is 1×10^{-4}, which means that 1.1° noise is contained into the observation.

The main structure of the prediction system is shown in Fig. 3. Under the interference of the complex environmental torque and the attitude orbit coupling, the angular velocity of the spacecraft changes irregularly. The attitude data are used as measurement samples for the torque identification and the attitude prediction algorithm verification. Figure 4 shows the real attitude and angular velocity of the spacecraft in LEO for 1 h. Figure 5 shows the Euler angle error in distribution diagram.
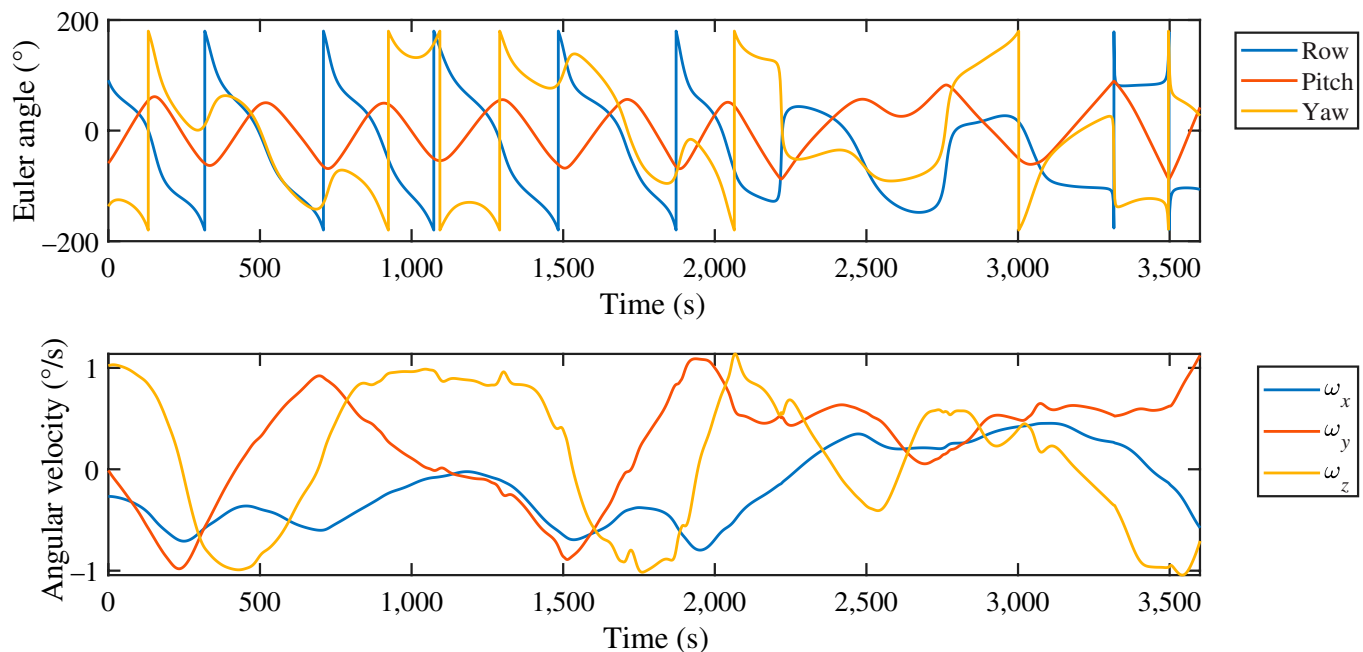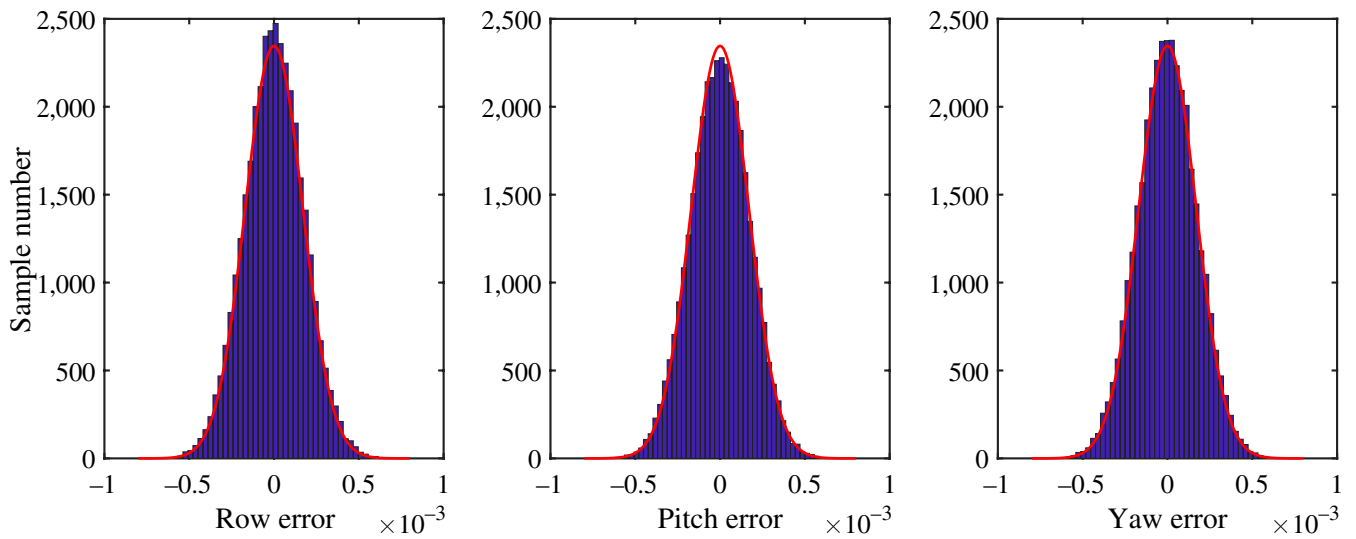

Fig. 4. The real Euler angle and angular velocity.

Fig. 5. Euler angle error in distribution diagram.

After a period of iteration, the tracking is extracted quickly. The identification results have strong shake since the ESO is highly based on the observation. However, these shakes are filtered out during the training of the neural network due to the independence between the attitude and the estimated results. The identification results are provided to the neural network according to the algorithm in the Unmodeled Compensation Based on Neural Network section. The neural network parameters used in this paper are set as: $N_1 = 6$, $N_2 = 6$, learning rate $\alpha = 0.1$, and maximum epoch is 200. The real torques, identification results, and network output are shown in Fig. 6. The yellow represents the identification results, the blue represents the real torque, and red represents the torque estimated by the trained neural network. The results show that the neural network can eliminate the shakes in the ESO and obtain high-precision estimation of the unmodeled dynamics. Besides, the activation function of the neural network has a great influence on the learning effect. The neural network with the "Relu+Sigmoid" activation function has better effect than other activation functions through simulations, such as the "Sigmoid+Relu", "Sigmoid+Sigmoid" function, etc.

Figure 7 shows the prediction effect of the whole system after compensation. The blue line represents the real attitude after 1 hour, the red line represents the attitude prediction results without neural network compensation, the yellow line represents the attitude prediction compensated by the neural network,
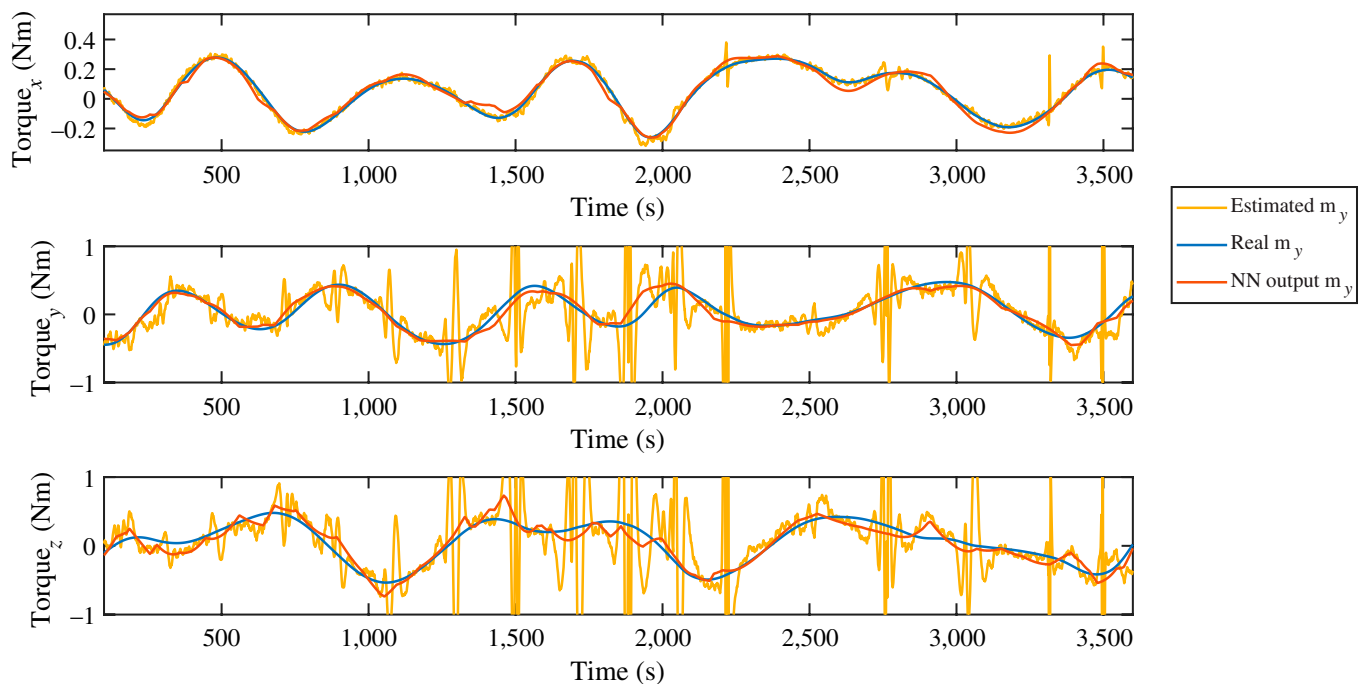

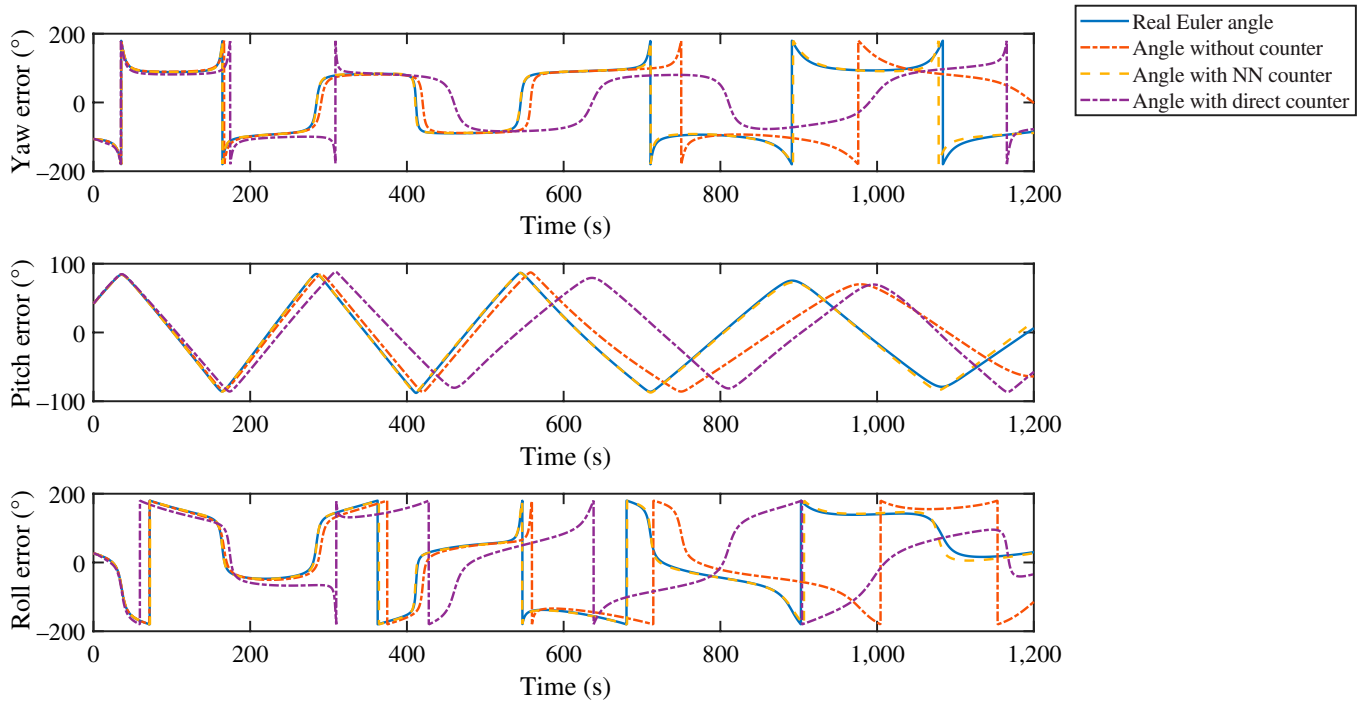**Fig. 6.** The real torque and neural network learning results.

Fig. 7. The prediction triaxial Euler angle with and without compensation.

while the purple line represents the attitude estimation generated by using the direct state estimation results, in which the error is large because of the interference of measurement noise. The comparison shows that the attitude estimation accuracy after compensation is higher and the accurate period is longer.

The final results of the proposed algorithm and the attitude determination results are presented in Fig. 8. The results show the observation error of the neural network compensated, directly compensated, and uncompensated prediction with the periodic observation correction (the cycle is 500 s). The comparison indicates that under the periodic observation correction, the spacecraft attitude prediction drift in the LEO exceeds 100° with directly compensation or without compensation, while the error is nearly controlled within 10° under the function of the neural network compensation, which demonstrates the effectiveness of the whole attitude compensation and prediction system.
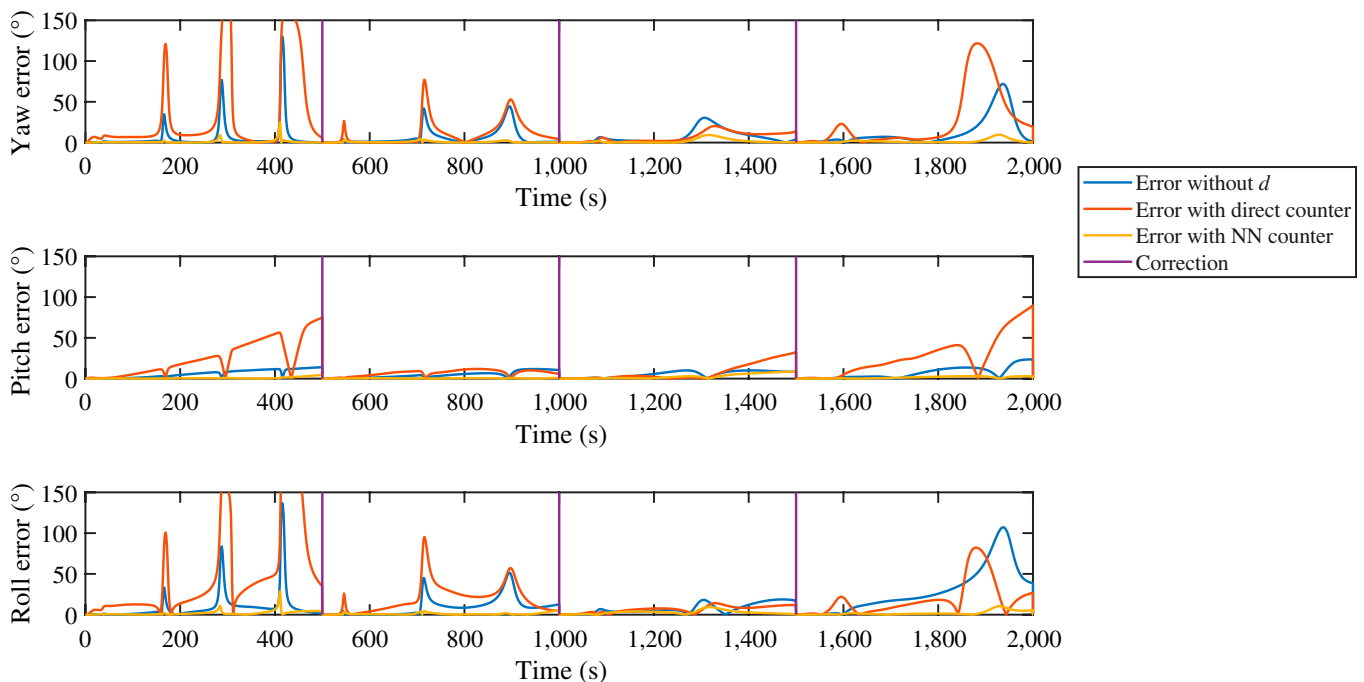

Fig. 8. The prediction triaxial Euler error with periodic observation correction.

Conclusion

Here, a novel prediction system is proposed to solve the attitude determination problem of the low-orbit malfunctioning satellite. An unmodeled torque identification method based on the quaternion is introduced. Then, an attitude prediction system is proposed combined with the BP neural network. The simulation results show that this method has high prediction accuracy and high reliability with discontinuous measurement, which proves the superiority and feasibility of this new method. In addition, this method has high expansibility and can be applied to various high-precision prediction fields with unmodeled disturbances. Excellent prediction results can be obtained easily by optimizing the identification algorithm and designing appropriate activation function.

Acknowledgments

Data Availability

The data used in the analysis and simulation are available from the corresponding author upon request.

References

1. Wang Y, Xu S. Gravity gradient torque of spacecraft orbiting asteroids. *Aircr Eng Aerosp Technol*. 2013;85(1):72–81.
2. Cilden-Guler D, Kaymaz Z, Hajiyev C. Geomagnetic disturbance effects on satellite attitude estimation. *Acta Astronaut*. 2021;180:701–712.
3. Guler DC, Kaymaz Z, Hajiyev C. Geomagnetic models at low Earth orbit and their use in attitude determination. Paper presented at: 2017 8th International Conference on Recent Advances in Space Technologies (RAST); 2017 June 19–22; Istanbul, Turkey.
4. Habila A. S. K. , Steyn W. H. In-orbit estimation of the slow varying residual magnetic moment and magnetic moment induced by the solar cells on cubesat satellites. Paper presented at: 2020 International Conference on Computer, Control, Electrical, and Electronics Engineering (ICCCEEE); 2021 Feb 26–01 March;Khartoum, Sudan. p. 1–6.
5. Schielicke L, Névir P. Introduction of an atmospheric moment combining eulerian and lagrangian aspects of vortices: Application to tornadoes. *Atmos Res*. 2011;100(4):357–365.
6. Shen H, Yu L, Jing X, Tan F. Method for measuring the second-order moment of atmospheric turbulence. *Atmos*. 2021;12(5):564.
7. Li Q, Yuan W, Zhao R, Wei H. Study on effect of aerodynamic configuration on aerodynamic performance of mars ascent vehicles. *Space Sci Technol*. 2022;2022:Article 9790131.
8. Crassidis JL, Markley FL, Cheng Y. Survey of nonlinear attitude estimation methods. *J Guid Control Dyn*. 2007;30(1):12–28.
9. Lam Q, Woodruff C, Ashton S, Martin D. Noise estimation for star tracker calibration and enhanced precision attitude determination. Paper presented at: Proceedings of the Fifth International Conference on Information Fusion. FUSION 2002. (IEEE Cat.No.02EX5997); 2002 July 8–11; Annapolis, MD. vol. 1:p. 235–242.
10. Xiong K, Liang T, Yongjun L. Multiple model Kalman filter for attitude determination of precision pointing spacecraft. *Acta Astronaut*. 2011;68(7-8):843–852.
11. Yang B, Huang H, Cao L. Centered error entropy-based sigma-point Kalman filter for spacecraft state estimation with non-Gaussian noise. *Space Sci Technol*. 2022;2022:Article 9854601.
12. Markley FL, Crassidis JL. *A predictive attitude determination algorithm*; Flight Mechanics Symposium; 1997. p. 249–263.
13. Iwata T, Hoshino H, Yoshizawa T, Kawahara T. Precision attitude determination for the advanced land observing satellite (alos): Design, verification, and on-orbit calibration. Paper presented at: AIAA Guidance, Navigation and Control Conference and Exhibit; 2007 Aug 20–23; Hilton Head, South Carolina.
14. Najder J, Sośnica K. Quality of orbit predictions for satellites tracked by SLR stations. *Remote Sens*. 2021;13(7):Article 1377.
15. Ovchinnikov MY, Ivanov DS, Ivlev NA, Karpenko SO, Roldugin DS, Tkachev SS. Development, integrated investigation, laboratory and in-flight testing of chibis-M microsatellite ADCS. *Acta Astronaut*. 2014;93:23–33.
16. Huang X, Li M, Wang X, Hu J, Zhao Y, Guo M, Xu C, Liu W, Wang Y, Hao C, et al. The Tianwen-1 guidance, navigation, and control for Mars entry, descent, and landing. *Space Sci Technol*. 2021;2021:Article 9846185.
17. Liang S, Srikant R. *Why deep neural networks for function approximation?* arXiv. 2016. https://doi.org/10.48550/arXiv.1610.04161
18. Lin C, Xiaoyu F, Santos R, Xu M. Intelligent fuzzy control in stabilizing solar sail with individually controllable elements. *Space Sci Technol*. 2022;2022:Article 9831270.
19. Carrara AV. Satellite attitude acquisition using a neural network controller. In: Prado ABA, editor. *Advances in space dynamics*; Advances in Space Dynamics; 2000. p. 272–282.
20. Zhang A, Liao Y, Ni S, Li Z, Yang X, Yan D. Simulation of satellite attitude control based on bp neural network. Paper presented at: 2021 6th International Conference on Intelligent Computing and Signal Processing (ICSP); 2021 April 9–11; Xi'an, China. p. 681–686.
21. Raja M, Singh K, Singh A, Gupta A. Design of satellite attitude control systems using adaptive neural networks. *Incas Bulletin*. 2020;12(3):173–182.
22. Yu ST,Fan CZ. Adaptive control of satellite attitude tracking based on RBF neural network. Paper presented at: 2020 5th International Conference on Automation, Control and Robotics Engineering (CACRE); 2020 Sep 19–20; Dalian, China.
23. Pisacane VL. *Fundamentals of space systems*. Johns Hopkins University Applied Physics Laboratories Series in Science and Engineering; 2005. p. 44–50.